# Effect of the properties of the surrounding gas on the dynamic behaviour of bouncing droplets on a solid surface

A. S. Moita*[1], N. Roth[2], H. Gomaa[2], B. Weigand[2] and A. L. N. Moreira[1]
*1: Instituto Superior Técnico, TU Lisbon, Av. Rovisco Pais, 1049-001 Lisbon, Portugal.
2: Institute of Aerospace Thermodynamics, Universität Stuttgart, Pfaffenwaldring 31, 70569 Stuttgart, Germany.

**Abstract**

Recent studies evidence the importance of the surrounding gas on the onset of several outcomes of droplet impact such as the *corona splash* and the rebound. However, additional research is still required to identify the thermo-physical properties which are relevant to the accurate description of the observed phenomena. In this context, the present paper addresses the investigation of the effect of the thermo-physical properties of the surrounding gas on the dynamic behaviour of micrometric liquid droplets impinging onto a solid surface at room temperature. The droplets impinge the surface with a very low angle, which introduces a non-negligible velocity component parallel to the surface, which promotes non-wetting conditions and consequent droplets rebound. The work considers the variation of the gas properties over a wide range, covering several conditions relevant for practical applications. Particular emphasis is given to the dynamic interaction between the droplet and the thin gas layer underneath it, during the rebound process, which is described in time, from a few instants (hundreds of μs) before impact until the moment at which the droplet lifts off the surface. This investigation is mainly numerical, since the simulations of the rebound were validated experimentally in a previous study, which was performed at atmospheric pressure, when the surrounding gas is air. The results show that increasing the density or the viscosity of the surrounding gas will increase the spacing between droplet and wall. This is related to the momentum transfer between the droplet and the surrounding gas, which alters the aerodynamic forces responsible for droplet bouncing. An important role is played by the velocity component parallel to the surface, which contributes to the motion of the air in the gap between the droplet and the surface and introduces significant velocity gradients in the air flow, increasing viscosity dissipation and contributing to the damping effect within the gas in the gap.

## Introduction

The accurate description of the dynamic behaviour of droplets impinging on a solid surface is a complex task which involves dealing with numerous parameters, namely the size and the velocity of the droplets, the thermo-physical properties of the liquid and of the solid, the wettability and the topography of the surface. Depending on the relative importance of these parameters, different outcomes can result from droplet impact, which are usually predicted based on empirical criteria, most of them function of the Weber, the Reynolds and the Ohnesorge number, as recently reviewed by Moreira *et al.* [1]. Actually, most of the authors use the Weber number to establish limiting conditions to distinguish four basic outcomes, namely the stick, the rebound, the spread and the ”splash”. In these studies the wall is wetted shortly after the droplet has approached the wall in all or at least most cases. The thermo-physical properties of the surrounding gas are often addressed to play a secondary role, so, most of the numerous models describing the rebound mechanism either on cold (*e.g.* Mao *et al.* [2], Okumura *et al.* [3]) or on heated surfaces (*e.g.* Aziz and Chandra [4]) do not take into account the effect of the gas properties. However, they cannot be disregarded. A recent work reported by Rein and Delplanque [5], Jepsen *et al.* [6] and Xu [7] show that a very thin layer of the surrounding gas, (whose thickness can be smaller than 3μm) is often entrained between the droplet and the surface at very late pre-impact instants and significantly affects the threshold of the disintegration mechanisms, namely of the *prompt splash* and of the *corona splash*. Xu [7,8] correlated a critical threshold pressure for the onset of the *corona splash* with the impact velocity. Mainly, his analysis revealed that a heavier surrounding gas and/or larger pressure will contribute to destabilize the action of the surface tension forces, thus favouring the onset of the *corona splash*. This is consistent with the analysis performed by Jepsen *et al.* [6], who argue, based on numerical simulations, that the lift up of the lamella, characteristic of the *corona splash* is favoured by the momentum that is transferred from this thin gas layer. Naturally, the wetting conditions are known to play a vital role in these processes. For instance, the rebound mechanism is promoted by non-wetting conditions. So, when the contact angle is high but the droplet still wets the surface (*e.g.* as reported in Mao *et al.*, [2]) the rebound only occurs as explained by Rein [9]: in the ab-

*Corresponding author: anamoita@dem.ist.utl.pt

sence of phase change, as the droplet impacts the surface, the liquid spreads radially, forming the lamella. At the maximum extent of the lamella, its free surface energy is quite high and strong surface tension forces pointing to the center cause the liquid to recoil into the core region. However, under non-wetting conditions, considered in the present study, the thin gas layer will be entrapped between the droplet and the surface and the pressure forces applied from this layer are so high that they will always promote the bouncing of the droplets.

In this scenario, the present work discusses the dynamic behaviour of micrometric liquid droplets impinging onto a solid surface at non-wetting conditions. The impaction occurs at a very low angle, so there is a non-negligible velocity component of the impinging droplet which contributes to its motion, parallel to the surface, over the gas layer underneath it (*e.g*. as in Karl *et al.* [10, 11]). Under these conditions, while droplet deformation is mainly due to the effect of the normal component of the impact velocity, the wetting is omitted by aerodynamic effects resulting on a promotion of the bouncing, (this mechanism will be discussed in the section *Results and discussion* of the present paper), which are investigated for a wide range of gas densities and viscosities. This dynamic interaction will determine the film thickness and pressure distribution of the gas layer underneath the droplet, which are described in time, from a few instants (hundreds of μs) before impact until the moment the droplet lifts off the surface.

Besides its relevance for a number of applications occurring at atmospheric pressure (*e.g.* coating processes) and in confined environments (*e.g.* in I.C. engines), this study is expected to provide useful information to cooling applications. For instance, in the metallurgical industry the quality of the final product requires a dedicated precise cooling for the casting and milling machines. In this case, an accurate description of the violent rebound process of the droplets which often occur as they impinge the surface within the film boiling regime (*i.e.* above the Leidenfrost temperature) is important to achieve a good overall cooling performance. In fact, there are differences between film boiling and the Leidenfrost regime, since in the film boiling regime the surface is wetted and as its temperature is above the boiling temperature of the liquid, it starts boiling at the surface, while in the Leidenfrost regime the surface is not wetted. The conditions studied in this paper are below the film boiling regime, so the non-wetting is due to aerodynamic effects. However, future investigations may confirm a superposition of the aerodynamic effects discussed here and Leidenfrost effect, which may explain the difficulties in defining a Leidenfrost regime for inclined droplet impact. Finally, the present study is also relevant to further understand the hydrodynamic and thermal behaviour of droplets impinging onto hydrophobic surfaces. Particularly, the analysis of the pressure distribution underneath the droplet during the bouncing process can be useful to apply, in future studies, to micro-textured surfaces, to understand the effect of the micro-textured pattern in the force balance during droplet-surface interaction, which ultimately will determine the wetting behaviour of the droplet over the wall. This approach is being explored in a few experimental works (*e.g.* Moita and Moreira [12], Varanasi *et al.* [13]) who established a threshold criterion to predict homogeneous or heterogeneous wetting and droplet recoil, based on a pressure-balance model.

**Materials and Methodologies**

This study investigates the effect of the surrounding gas on the rebound of ethanol droplets, at room temperature. The present paper will only address the numerical study. Simulations obtained for similar impact conditions were early validated experimentally, as in Roth *et al.* [14].

Mainly, the test cases consider the variation of the specific mass and of the dynamic viscosity of the surrounding gas, which are the properties more likely to be related with the dynamic behaviour of the impinging droplets. So, the dynamic viscosity of the surrounding gas $\mu_g$ is varied between $0.5\mu_{g0}$ and $3\mu_{g0}$, while its specific mass, $\rho_g$ is varied between $\rho_{g0}$ and $3\rho_{g0}$, where $\rho_{g0}$=1.205kg/m$^3$ and $\mu_{g0}$=1.837x10$^{-5}$kg/(ms) are, respectively the density and the dynamic viscosity of air, at 20ºC and atmospheric pressure.

The impact conditions are fixed within the values presented in Table 1. Table 2 summarizes the range of thermo-physical properties of the liquids and gases used in this study.

**Table 1.** Impacting parameters used in the study. The parameters are defined as in Figure 1.

| **Impact parameters** | **Range** |
|---|---|
| Diameter of the primary droplets - $D_0$ [μm] | 180 |
| Impact velocity - $\upsilon_0$ [m/s] | 10 |
| Spacing between consecutive droplets – s [μm] | 600 |
| Impaction angle - α [º] | 2 |
| Surface temperature – $T_w$ [ºC] | 20 |

**Table 2.** Range of the thermo-physical properties of the liquids and gases used in the study. The subscripts *l* and *g* refer to the liquid droplet and to the surrounding gas, respectively.

| **Thermo-physical properties of Ethanol (@20ºC and atmospheric pressure)** | **Range** |
|---|---|
| Specific mass - $\rho_l$ [kg/m$^3$] | $\rho_l$=788.5 |
| Dynamic viscosity - $\mu_l$ [kg/(ms)] | $\mu_l$ =1.0x10$^{-3}$ |
| Surface tension – $\sigma$[N/m] | $\sigma$=22.5x10$^{-3}$ |
| **Thermo-physical properties of the surrounding gas** | **Range** |
| Specific mass - $\rho_g$ [kg/m$^3$] | $\rho_{g0}\leq\rho_g\leq3\rho_{g0}$ , with $\rho_{g0}$=1.205 |
| Dynamic viscosity - $\mu_g$ [kg/(ms)] | $0.5\mu_{g0}\leq\mu_g\leq3\mu_{g0}$, with $\mu_{g0}$=1.837x10$^{-5}$ |

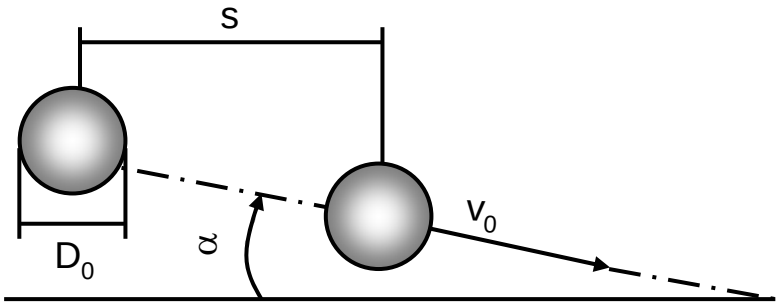


**Figure 1.** Schematic representation of the impact parameters. $D_0$ and $\upsilon_0$ are the initial diameter and impact velocity of the droplets, whereas s is the spacing between two consecutive droplets in the stream and $\alpha$ is the impaction angle.

Here, s is the spacing between the droplets, which are produced by a monodisperse droplet generator. The angle $\alpha$ and $v_0$ are respectively the impact angle and impact velocity of the droplets, defined as in Figure 1. The subscripts *l* and *g* refer to the liquid droplet and to the surrounding gas, respectively.

The impact conditions are chosen to assure that the surface is not wetted.

**Numerical Method**

The 3D CFD program FS3D, developed at the ITLR, was specially developed to compute the Navier Stokes Equations for incompressible flows with free surfaces using Direct Numerical Simulation (DNS). The flow field is computed by solving the governing equations for mass conservation and momentum conservation

$$\rho_t + \nabla\cdot(\rho\mathbf{u}) = 0 \tag{1}$$

$$(\rho\mathbf{u})_t + \nabla\cdot((\rho\mathbf{u})\otimes\mathbf{u}) = \nabla\cdot(\mathbf{S}-\mathbf{I}p) + \rho\mathbf{g} + \mathbf{f}_\gamma \tag{2}$$

Here $\mathbf{u}$ denotes the velocity, $\rho$ the density, $p$ the static pressure and $\mathbf{g}$ the acting volume forces. The stress tensor is formulated for Newtonian fluids by $\mathbf{S} = \mu\left(\nabla\mathbf{u} + (\nabla\mathbf{u})^T\right)$, where $\mu$ is the dynamical viscosity. The surface tension force, which is stated by the capillary stress tensor $\mathbf{f}_\gamma$ is handled as a volume force that acts on every cell containing an interface. Due to the mentioned incompressibility and the assumed constant fluid properties in each phase the energy equation is decoupled from the momentum equation and not solved within this study. To describe the interface between the liquid and gaseous phase that are assumed to be inert, the Volume of Fluid (VOF) method by Hirt and Nichols [15] is used. Here an additional variable $f$, specifying the liquid volume fraction, is introduced as follows

$$f(\mathbf{x},t)=\begin{cases}0 & \text{within the gaseous phase}\\ [0;1] & \text{along the interface cells}\\ 1 & \text{within the liquid phase}\end{cases} \tag{3}$$

This allows for a concise one field formulation where from simple scaling the properties of the gas and the liquid, the density and viscosity field, might be calculated to

$$\rho(\mathbf{x},t)=\rho_g+(\rho_f-\rho_g)f(\mathbf{x},t) \tag{4}$$

$$\mu(\mathbf{x},t)=\mu_g+(\mu_f-\mu_g)f(\mathbf{x},t) \tag{5}$$

To describe the temporal and spatial evolution of the volume fraction $f$ an additional transport equation, analogously to Eq.(1), is defined by

$$f_t+\nabla\cdot(f\mathbf{u})=0 \tag{6}$$

The presented equations are discretized by finite volume schemes with an accuracy of second order in space on a staggered grid. In time the equations are integrated by the implicit second order Crank-Nicolson scheme. The calculation of the fluxes in Eq.(6) is based on a piecewise linear reconstruction of the interface in each cell, the so called piecewise linear interface reconstruction (PLIC) method proposed by Rider and Kothe [16], which ensures a sharp interface and widely suppresses numerical dissipation. The Poisson equation for the pressure resulting from the assumption of incompressibility is solved by a multigrid solver that uses Red-Black Gauss Seidel as smoothing algorithm. The number of pre- and post- smoothing steps in V and W cycles is adopted during runtime by means of the corresponding residuals allowing for optimized computation times. The whole code is vectorized as well as parallelized, featuring the possibility of large computational domains on the vector computers of The High Performance Computing Center Stuttgart (HLRS). FS3D also allows for the consideration of the temperature field and the evaporation of the liquid phase, which is not considered here. An overview of the possibilities of FS3D is given by Gomaa *et al.* [17].

The geometry considered in the simulations is schematically represented in Figure 2.

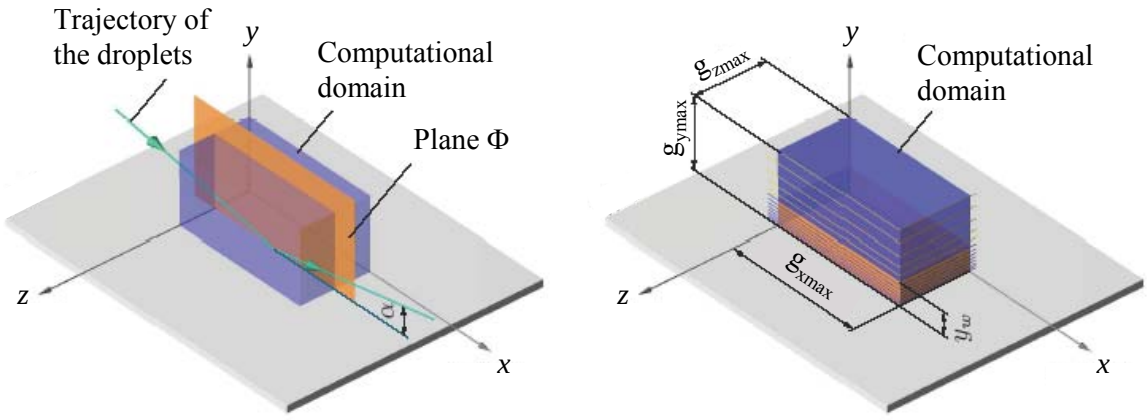


**Figure 2.** Geometric arrangement used in the simulations. Adapted from Roth *et al.* [14].

The bottom of the computational domain is the target wall. Plane Φ, which is perpendicular to the impact surface, is defined by the trajectory of the incoming and of the reflected droplets. The intersection between this plane and the surface defines the *x*-direction. The width of the computational domain is defined by: $g_{xmax}$=600µm, $g_{ymax}$ =300µm and $g_{zmax}$=300µm. A rectangular grid is used, with refinements near the surface. The grid cells are equidistant in the *x* and in the *z*-directions. The number of grid cells in the *x* and in the *z* directions are, respectively $n_x$=256 and $n_z$=128. In the *y*-direction the computational domain is divided in two sec-

tions: a lower section for $0 \leq y \leq y_w = 100\mu m$, with $n_{yu}=48$ grid cells and an upper section for $y_w \leq y \leq g_{ymax} = 100\mu m$ with $n_{yr}=80$grid cells. The total number of grid cells in the *y*-direction is $n_y = n_{yu} + n_{yr}=128$. The plane with the smallest grid cells is located directly at the wall with the height $\Delta_y(1)=0.625\mu m$. The height of the grid cells increases in the direction of increasing y-values. The difference in height between neighbouring grid cells is constant, within each of the two sections in which the computational domain was divided.

Regarding the boundary conditions, the no-slip condition was applied at the bottom of the computational domain. The other three sides, which are parallel to the *x*-direction, von Newman conditions were used. It is worth noting that during the bouncing process, no liquid mass passes these three boundaries. For the remaining sides perpendicular to the *x*-direction periodic conditions were used, to simulate the monodisperse stream of droplets. Therefore, liquid mass leaving the computational domain at $x=g_{xmax}$ will immediately enter again the domain at $x=0$. The simulations are performed fully 3D, without any symmetry assumptions. A more detailed description of the numerical method is given in Gomaa *et al.* [17].

**Results and discussion**

Under the specific impact conditions presented in Table 1, namely considering the small impinging angle used here, the droplet will not wet the surface and therefore will rebound after impact. As briefly explained in the introduction, the rebound is governed by two mechanisms, which are related to the liquid surface tension and to the aerodynamic forces induced by droplet motion. This interaction can be interpreted by analysing the temporal evolution of the minimum thickness of the gas gap between the droplet and the surface, as represented in Figure 3, when the gas has $\mu_g=\mu_{g0}$ and $\rho_g=\rho_{g0}$. The gap between droplet liquid and wall has a very complex structure, which has been shown in [14,18] So, the air is accelerated beneath the impinging droplet generating a pressure force close to the wall. As the droplet spreads and travels in the radial direction (parallel to the wall), momentum is transferred from the vertical to the horizontal direction so that the air underneath, by mass conservation, and considering that the flow is incompressible, moves towards the horizontal direction. Consequently, the distance in the gap between the droplet and the surface is minimal (*e.g.* at t=5.1E-5s in Figure 3). Following this argument, the pressure force on the wall should depend, by mass and momentum conservation within the gas gap, on the deformation area (or radius) of the droplet and on the gas density.

Afterwards, the thickness of the gas layer recovers a larger distance, as at this stage the droplet will only slightly spread, in a deformation process which is mainly associated to the normal component of the impact, whereas the velocity component parallel to the wall and the shape of the droplets promotes a lift force. (*e.g.* for 5.1E-5s<t<3.8E-4, in Figure 3). During this stage, kinetic energy converted in surface tension energy, while part can be dissipated to the air, so that one should not observe a perfect reflection. After maximum deformation is achieved, retraction of the liquid takes place driven by surface tension. The retracting droplet reaches its minimum contact with the gas before it bounces (*e.g.* t>4.14E-4s).

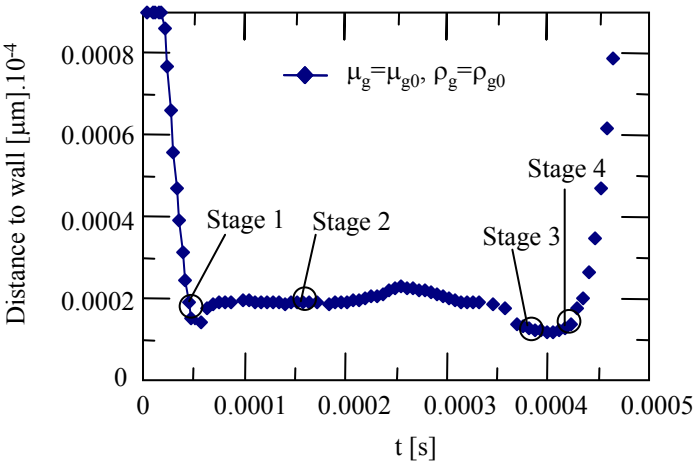


**Figure 3.** The temporal evolution of the distance between an impacting ethanol droplet ($D_0=180\mu m$, $v_0=10m/s$, $\alpha=2°$) and a smooth surface. The simulations were performed for $\mu_g=\mu_{g0}$ and $\rho_g=\rho_{g0}$.

The topology of the droplet within the various stages described above is represented in Figure 4.

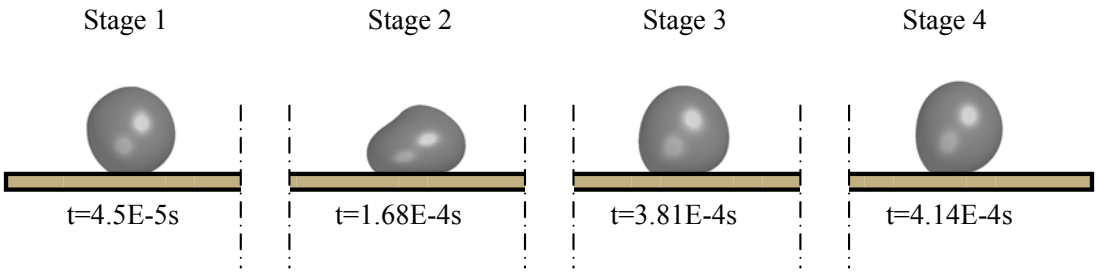


**Figure 4.** Numerical prediction of the temporal evolution of the morphology of an ethanol droplet ($D_0$=180μm, $v_0$=10m/s, α=2º) impinging on a smooth surface. The simulations were performed for the condition $\mu_g=\mu_{g0}$ and $\rho_g=\rho_{g0}$.

Here, one may see the behaviour of the droplet at the initial stage of impact, at the stage of spreading, while travelling over the gas layer (when the distance between the droplet and the surface is maximum) and at the stage when the droplet starts to apart from the surface and its distance to the surface starts to raise substantially. The distance between the surface and the droplet cannot be seen in the Figures since it is too small.

In agreement with this description, the pressure forces acting on the wall, as represented in Figure 5, increase substantially at droplet impact, further decreasing gradually during the lift of the droplet, until zero (when it completely bounces off the surface).

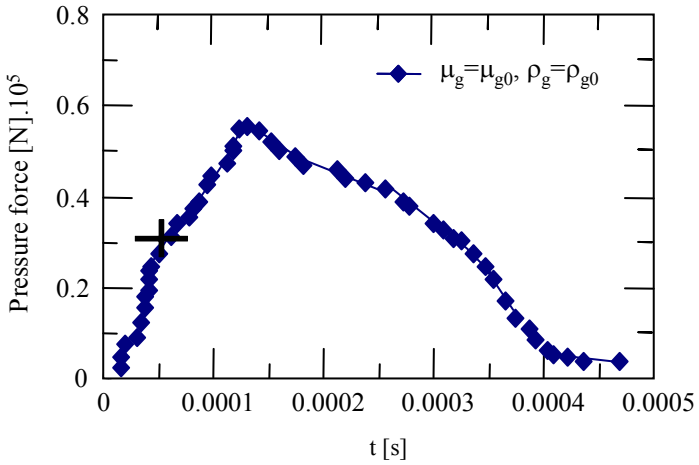


**Figure 5.** Computation of the pressure forces acting on the wall during the rebound process of an ethanol droplet ($D_0$=180μm, $v_0$=10m/s, α=2º) impacting on a smooth surface, for $\mu_g=\mu_{g0}$ and $\rho_g=\rho_{g0}$. The + indicates the exact instant at which the distance between the droplet and the surface is minimum at the beginning of the impact.

In line with this, the pressure distribution on the droplet surface and the corresponding forces acting on the droplet, (namely lift, drag and side force perpendicular to the plane defined by the trajectories of the droplet), as depicted in Figures 6 and 7 should also be consistent with the previous description. Once again, all the calculations presented here were performed for $\mu_g=\mu_{g0}$ and $\rho_g=\rho_{g0}$.

It is worth noting that the scales for the images in Figure 6 are different between the Figures, to provide a clearer view of the pressure distribution.

Looking at these Figures one may confirm that the view from the bottom actually corresponds quite well with the distribution of the pressure at the wall and with the distance between the droplet and the wall, presented in Figures 3 and 5. The side pressure force (perpendicular to the plane defined by the trajectories of the droplet) is almost zero within the whole rebound process, since the droplet configuration is symmetric.

On the other hand, the lift is quite similar to the pressure force on the wall, but there are some visible differences. A grounded explanation for this small discrepancy requires further calculations, to be developed in a future work.

Given that the non-wetting of the surface and the lift of the droplet result from aerodynamic forces, as described up to now, they should be influenced by the properties of the gas, namely its density and its viscosity. In line with this, Figures 8 and 9 depict the temporal variation of the distance between the droplet and the surface as well as the pressure force on the wall for various gas densities. The Figures show that increasing the gas density

increases the distance between the droplet and the surface, thus promoting its rebound. As the density of the gas increases, the volume of the gas layer accelerated within the horizontal direction decreases, so the positions of the minimum distance between the surface and the droplet increases. The pressure increases with the density thus favouring the lift off the droplet.

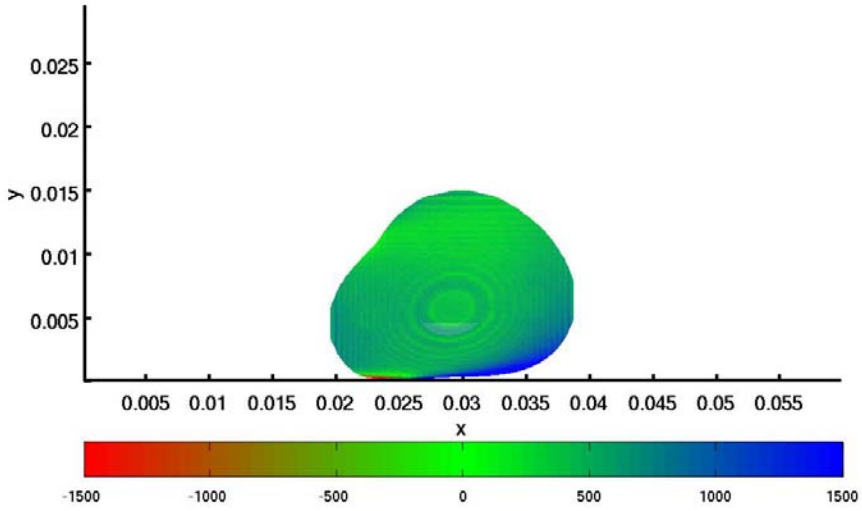


a)

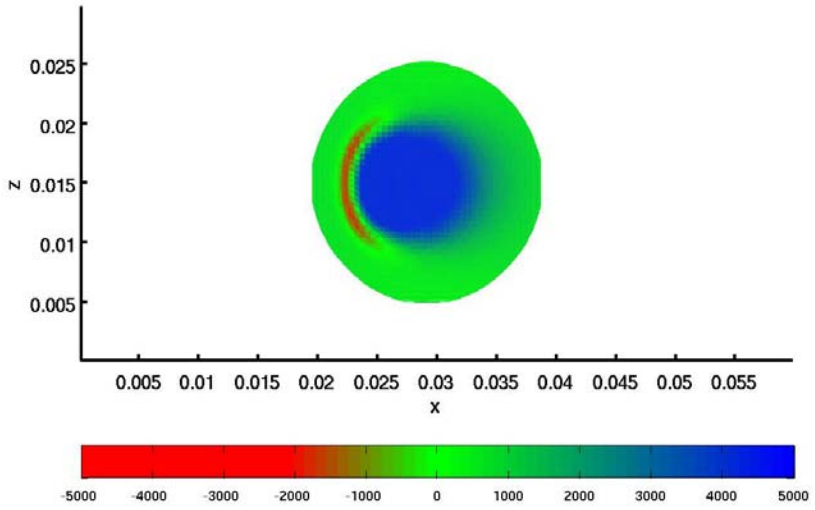


b)

**Figure 6.** Pressure distribution on the droplet, for $\mu_g=\mu_{g0}$ and $\rho_g=\rho_{g0,}$ when the region at which the spacing between droplet liquid and wall that is below 9μm has its largest extent: a) side view, b) bottom view. The rings in the side view are caused by interpolation effects.

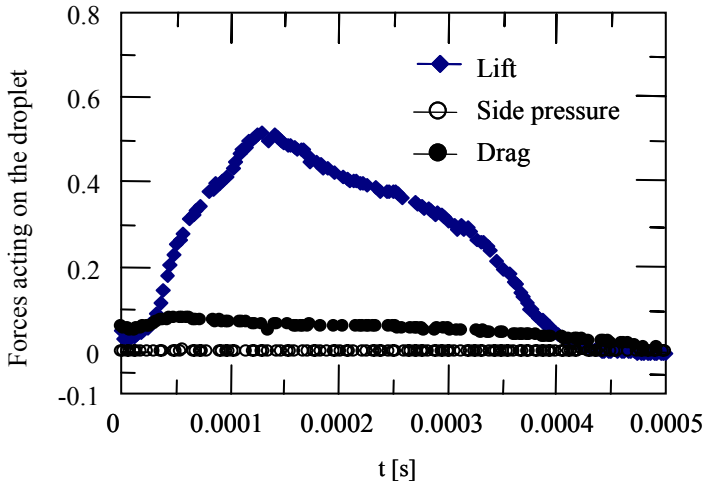


**Figure 7.** Pressure distribution on the droplet, for $\mu_g=\mu_{g0}$ and $\rho_g=\rho_g$.

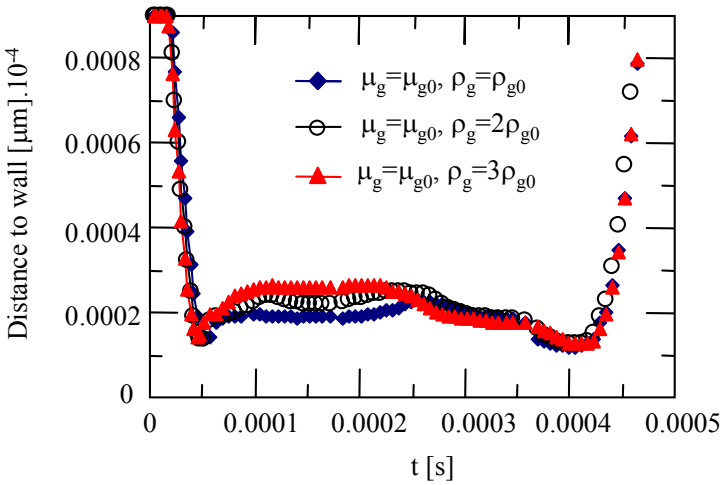


**Figure 8.** Effect of the gas density on the temporal evolution of the distance between an impacting ethanol droplet ($D_0$=180μm, $v_0$=10m/s, α=2°) and a smooth surface.

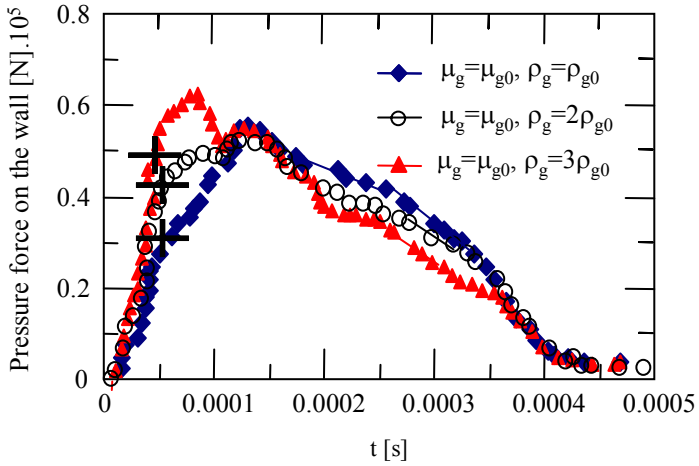


**Figure 9.** Effect of the gas density on the pressure forces acting on the wall during the rebound process of an ethanol droplet. The + indicates the exact instant for each tested condition, at which the distance between the droplet and the surface is minimum at the beginning of the impact.

The effect of gas viscosity is shown in Figures 10 and 11. At small impacting angles such as that used in the present work, the velocity component parallel to the surface introduces significant velocity gradients in the air

flow, increasing viscosity dissipation and contributing to the damping effect within the gas gap. This damping effect is enhanced for higher gas viscosities thus raising the distance between the droplet and the surface

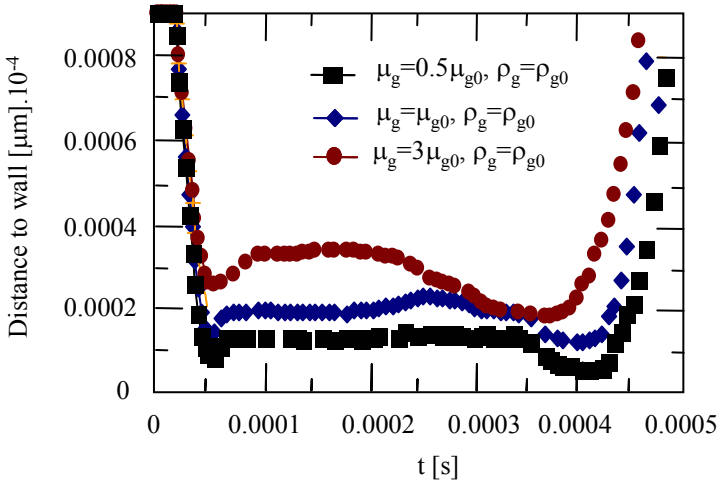


**Figure 10.** Effect of the gas viscosity on the temporal evolution of the distance between an impacting ethanol droplet ($D_0$=180μm, $v_0$=10m/s, α=2°) and a smooth surface.

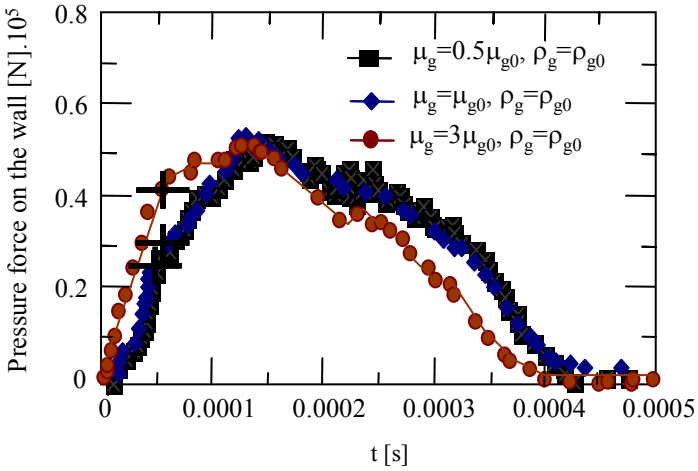


**Figure 11.** Effect of the gas viscosity on the pressure forces acting on the wall during the rebound process of an ethanol droplet ($D_0$=180μm, $v_0$=10m/s, α=2°) impacting on a smooth surface. The + indicates the exact instant for each tested condition, at which the distance between the droplet and the surface is minimum at the beginning of the impact.

## Conclusions

The present paper addresses the investigation of the effect of the thermo-physical properties of the surrounding gas on the dynamic behaviour of micrometric liquid droplets impinging onto a solid surface at room temperature. The droplets impact the surface with a very low angle, which introduces a non-negligible velocity component parallel to the surface, which promotes non-wetting conditions and consequent droplet rebound. Particular emphasis is given to the dynamic interaction between the droplet and the thin gas layer underneath it, during the rebound process, which is described in time, from a few instants (hundreds of μs) before impact until the moment at which the droplet lifts off the surface. The results evidence that increasing the density or the viscosity of the surrounding gas will increase the spacing between droplet and wall. This is related to the momentum transfer between the droplet and the surrounding gas, which alters the aerodynamic forces responsible for droplet bouncing. The velocity component parallel to the surface introduces significant velocity gradients in the air flow in the gap between the droplet and the surface, increasing viscosity dissipation and contributing to the damping effect within the gas in the gap. This study gives a first impression of the physical processes and is a first step in the development of a model based on the physics. Further studies will be performed to detail the processes discussed here, namely to understand the differences observed between the lift and the pressure force beneath the droplet. Once the physical processes governing the mechanisms which enlarge or reduce the gap between droplet liquid

and the surface are well described one may also predict the probability of the droplet to wet or non-wet the surface, when this is not smooth anymore.

**Acknowledgements**

The authors greatly appreciate the High Performance Computing Center Stuttgart (HLRS) for support and supply of computational time on the NEC-SX9 platform under the Grant No. FS3D/11142.

A. S. Moita also acknowledges the contribution of Fundação para a Ciência e a Tecnologia (FCT) by supporting her with a post-Doc Fellowship (Ref:SFRH/BPD/63788/2009).

**References**

[1] Moreira, A. L. N., Moita, A. S., Panão, M. R., *Progress in Combustion and Energy Sci.* 36:554-580 (2010).
[2] Mao, T., Kuhn, D. C. S., Tran, H., *AIChE Journal*, 43(9):2169-2179 (1997).
[3] Okumura, K., Chevy, F., Richard, D., Quéré, D., Clanet, C., *Europhysics Letters*, 62(2) :237-243 (2003).
[4] Aziz, S. D., Chandra, S. *Int. J. Heat Mass Transf.*, 43: 2841-2857 (2000).
[5] Rein, M., Delplanque, J.-P., *Act Mech.* 201:105-118 (2008).
[6] Jepsen, R.A., Yoon, S.S., Demosthenous, B., *19th ILASS Americas*, Toronto, Canada (2006).
[7] Xu, L., Zhang, W. W., Nagel, S. R., *Phys. Rev. Letters*, 94:184505 (2005).
[8] Xu, L., *Physical Rev. E* 75:056316 (2007).
[9] Rein, M., In: *Drop-Surface Interactions*, Edited by Martin Rein, SpringerWienNewYork (2002).
[10] Anders, K., Roth, N., Frohn, A. *Exp Fluids 15:91-96* (1993).
[11] Karl, A., Frohn, A., *Phys. Fluids*, 12(4):785-796 (2000).
[12] Moita, A. S., Moreira, A. L. N. *15th Int. Symp. Appl. Laser Tech. Fluid Mech.*, Lisbon, Portugal, July 2010.
[13] Varanasi, K. K., Paxson, A., Smyth, K., Kwon, H., *In: Proc. of the ASME IHTC14*, Washington, USA, August 2010.
[14] Roth, N., Gomaa, H., Bordoni, N., Dumont, T., Weigand, B., *23rd ILASS-Europe*, Brno, Czech Republic, September 2010.
[15] C. W. Hirt, B. D. Nichols, *Journal of Computational Physics*, 39:201-225 (1981).
[16] W.J. Rider, D. B. Kothe., *Journal of Computational Physics*, 141:112-152 (1998).
[17] Gomaa, H., Roth, N., Schlottke, J., Weigand, B., *Atomization and Sprays*, 20(4): 281-296 (2010).
[18] Roth, N., Schlottke, J., Urban, J., Weigand, B., *22nd ILASS-Europe*, Como, Italy, September 2008.